ACS SyntheticBiology

Research Article

pubs.acs.org/synthbio

Repurposing *Synechocystis* PCC6803 UirS−UirR as a UV-Violet/Green Photoreversible Transcriptional Regulatory Tool in *E. coli*

Prabha Ramakrishnan[†] and Jeffrey J. Tabor*[,†,‡]

[†]Department of Bioengineering, [‡]Department of Biosciences, Rice University, 6100 Main Street, Houston, Texas 77005, United States

Supporting Information

ABSTRACT: We have previously engineered green/red and red/far red photoreversible *E. coli* phytochrome and cyanobacteriochrome (CBCR) two-component systems (TCSs) and utilized them to program tailor-made gene expression signals for gene circuit characterization. Here, we transport the UV-violet/green photoreversible CBCR TCS UirS−UirR from *Synechocystis* PCC6803 to *E. coli*. We demonstrate that the promoter of the small RNA *csiR1*, previously shown to be activated by inorganic carbon stress, is a UirS−UirR output. Additionally, in contrast to a recently proposed sequestration model, we show that the sensor histidine kinase UirS phosphorylates the response regulator UirR to activate P_{csiR1} transcription in response to UV-violet light. Finally, we measure changes in UirS−UirR output minutes after a change in light input and exploit these rapid dynamics to program a challenging gene expression signal with high predictability. UirS−UirR is the first engineered transcriptional regulatory tool activated exclusively by UV-violet light, and the most blue shifted photoreversible transcriptional regulatory tool.

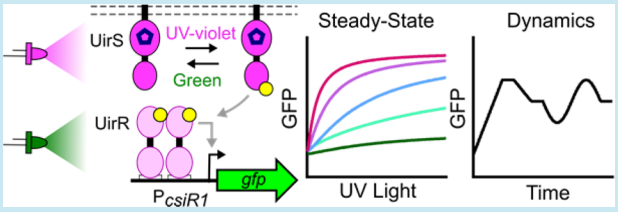

KEYWORDS: *optogenetics, bacterial two-component system, UV-violet light, light-regulated gene expression*

Optogenetics is a rapidly advancing technology wherein light and genetically encoded photoreceptors are used to control molecular biological processes in live cells or organisms. Because photons can be applied more precisely in the concentration, time, and space dimensions than traditional effectors such as chemicals, optogenetics enables unprecedented perturbations that can reveal new insights into biological function.[1] For example, researchers have recently used light-switchable gene expression, protein localization, and ion channel systems to advance understanding of gene circuit dynamics,[2] cell signaling pathways,[3] cellular differentiation,[4] and neural function.[5]

Two-component systems (TCSs) are the primary means by which bacteria sense and respond to environmental signals.[6] The classical TCS comprises a membrane-bound sensor histidine kinase (SK), a cytoplasmic response regulator (RR), and one or more output promoters. SKs are produced in a ground state that typically exhibits low kinase activity toward the RR, although there are notable exceptions with high ground state activity.[7] For a given SK, a specific chemical or physical input triggers a structural rearrangement at an N-terminal sensor domain that is transmitted to a C-terminal signaling domain. In this activated state, the signaling domain uses ATP to autophosphorylate a conserved histidine and the phosphoryl group is transferred to a conserved aspartate within an N-terminal receiver (REC) domain on the RR. REC domain phosphorylation drives a structural rearrangement that is transmitted to a C-terminal effector domain, frequently a DNA-binding domain (DBD), that then regulates gene expression.

Many TCSs sense light via Phytochrome superfamily sensor domains.[8] Phytochromes (Phys) and the related cyanobacteriochromes (CBCRs) absorb light via a covalently ligated linear tetrapyrrole (bilin) chromophore.[9] Phy and CBCR SKs are produced in a dark-adapted ground state. While ground-state Phys typically absorb red light,[9] different ground-state CBCRs exhibit varied maximal light absorbance wavelengths (λ_{max}) from the ultraviolet (UV) (334 nm)[10] to the red (652 nm).[11] Absorption of an appropriate photon triggers the chromophore to isomerize, which drives the photosensory domain to rapidly switch to an activated state. Activated Phys and CBCRs are also light sensitive, but they typically exhibit red-shifted wavelength sensitivities. Absorption of a deactivating photon drives rapid reversion to the ground state.

Previously, we engineered red/far-red (Phy)[12] and green/red (CBCR)[13] photoreversible TCSs in *E. coli* and used them for characterization and control of synthetic gene circuits.[2,14] The photoreversibility of these sensors enables more precise control of transcription rate and faster response dynamics.[2] We have exploited these features to program quantitatively and temporally defined gene expression signals, which can be used to characterize gene circuit dynamics *in vivo*.[2] Furthermore, we improved the performance and ease of use of each sensor by combining all necessary genes onto two plasmids from which we optimized expression of each SK and RR.[15]

Received: February 22, 2016
Published: April 27, 2016

DOI: 10.1021/acssynbio.6b00068
ACS Synth. Biol. 2016, 5, 733−740

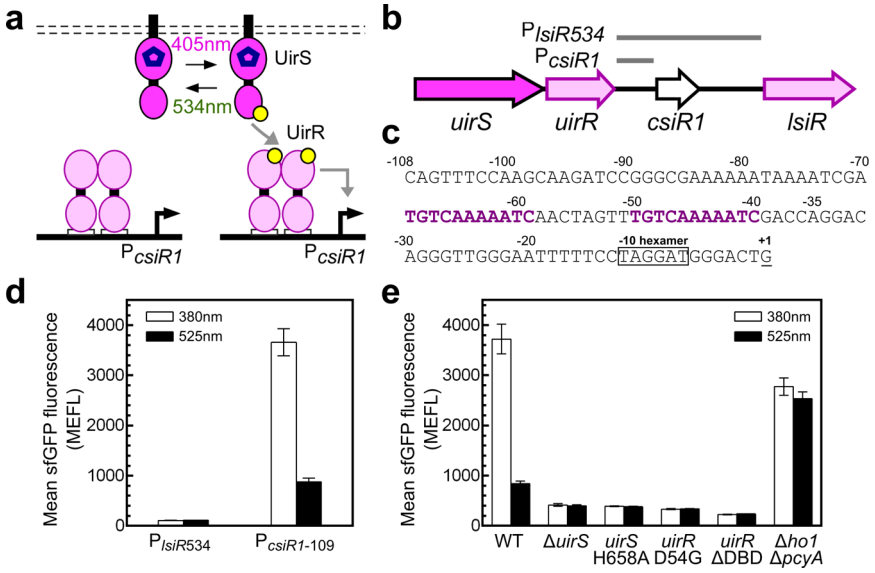

Figure 1. UV-violet/green photoreversible CBCR TCS UirS−UirR. (a) On the basis of the results of this study, we propose that UV-violet light switches PVB (blue pentagon)-ligated UirS from the ground state (P_{UV}) to the active state (P_g), enhancing autophosphorylation and phosphotransfer to UirR. UirR~P activates transcription from P_{csiR1}. Green light switches UirS back to P_{UV}. UirR is bound to its operator independent of phosphorylation state. (b) The *uirS/uirR/csiR1/lsiR* genomic region in *Synechocystis* PCC6803. (c) $P_{csiR1\text{-}109}$ sequence. The *csiR1* +1[20,22] is underscored and highlighted. The putative UirR half-sites are highlighted in bold, purple text. (d) Mean sfGFP fluorescence (in molecules of equivalent fluorescein; see Methods) of *E. coli* BW29655/pPR161-2/pPR157-1 ($P_{lsiR534}$) and BW29655/pPR161-2/pPR164-1 ($P_{csiR1\text{-}109}$) illuminated with 1.25 μmol m^{-2} s^{-1} 380 or 525 nm light and supplemented with 100 ng/mL aTc and 200 μM IPTG to induce *uirR* and *uirS* expression. Bar heights represent the arithmetic mean of flow cytometry fluorescence distributions. Error bars represent the standard error of the mean (SEM) of n = 3 experiments on separate days. (e) Mean sfGFP fluorescence of *E. coli* BW29655/pPR161-2/pPR164-1 (WT) and mutation controls. Light and inducer conditions are as in panel d. The modifications to WT are as follows: deletion of the UirS expression unit (Δ*uirS*), mutagenesis of the UirS catalytic histidine (UirS H658A), in-frame deletion of UirR amino acids 123−237 (*uirR*ΔDBD), mutagenesis of the UirS receiver aspartate (UirR D54G), and deletion of the chromophore expression unit (Δ*ho1*/Δ*pcyA*). sfGFP values and error bars are as in panel d.

In response to UV-violet (380−420 nm) light, the *Synechocystis* PCC6803 TCS UirS−UirR (Figure 1a) was recently shown to activate transcription of the adjacent output gene *lsiR* (Figure 1b), encoding a second RR involved in negative phototaxis.[16,17] The membrane-bound[18] CBCR SK UirS binds PCB and converts it to the blue-shifted isomer phycoviolobilin (PVB). Holo-UirS is produced in a low signaling ground state (P_{UV}) with a λ_{max} between 382[16] and 405 nm.[19] UV-violet switches UirS P_{UV} to an activated state (P_g) that reverts to P_{UV} in green (λ_{max} = 534 nm).[16] The RR UirR has a canonical REC domain and an AraC-family DBD.

However, UirS−UirR remains poorly understood, limiting optogenetic applications. First, the output promoter is not well characterized. *In vitro* experiments have shown that UirR binds upstream[16] of the low inorganic carbon (C_i)-induced non-coding RNA *csiR1*,[20] which resides between *uirR* and *lsiR* (Figure 1b). *csiR1* and *lsiR* are cotranscribed from the *csiR1* transcriptional start site (+1)[20−22] in a manner induced by low C_i.[23] However, *csiR1* expression has not been shown to be activated by UV-violet light nor UirR. Additionally, although UirS and UirR carry the conserved histidine and aspartate residues and the UirR aspartate is essential for negative UV-violet phototaxis,[16] autophosphorylation of UirS and phosphotransfer to UirR were not detected *in vitro*.[16,17] This fact, in combination with a measurable physical interaction between the UirS signaling and UirR REC domains,[16] led to a hypothesis wherein UirS P_{UV} sequesters UirR at the membrane, maintaining low transcriptional output in dark or green light. UV-violet induced switching to the UirS P_g form is then thought to result in liberation of UirR. Free UirR would then become phosphorylated to UirR~P by an agent other than UirS (such as acetyl phosphate), bind DNA, and activate transcription.[16] Because the UirS−UirR signaling mechanism may fundamentally differ from that of our previous sensors, it is unknown whether UirS−UirR can be used for similarly precise gene expression programming.

Here, we engineer UirS−UirR to function in *E. coli*, characterize its signaling mechanism and input/output properties, and utilize it to program tailor-made gene expression signals. First, we demonstrate that the *csiR1* promoter (P_{csiR1}) is a bona fide UirS−UirR output and characterize the UirR operator region. Then, we use a combination of mutations, variable UirS and UirR expression levels, and *in vivo* phosphorylation measurements to show that UirS phosphorylates UirR to activate transcription from P_{csiR1}, in contrast to the sequestration model. Third, we characterize the UirS−UirR action spectrum and demonstrate that it is activated by only UV-violet light. Finally, we experimentally characterize and mathematically model the UirS−UirR input/output dynamics and design a time-varying light signal that programs a complex gene expression waveform with high predictability. Our results yield new insights into the biology of UirS−UirR, establish it as the most blue-shifted photoreversible bacterial optogenetic tool and the only tool that is activated exclusively by UV-violet light, and demonstrate that it has performance features comparable to those of our green/red and red/far red sensors.

RESULTS AND DISCUSSION

Transporting UirS−UirR into *E. coli*. We constructed a two-plasmid system (Figure S1) from which *uirS* and *uirR* transcription can be induced with isopropyl β-D-1-thiogalactopyranoside (IPTG) and anhydrotetracycline (aTc), the PCB

DOI: 10.1021/acssynbio.6b00068
ACS Synth. Biol. 2016, 5, 733−740

biosynthetic operon *ho1-pcyA* is expressed constitutively, and the superfolder GFP[24] gene *sfgfp* is encoded downstream of the 534 bp *uirR/lsiR* intergenic region (hereafter $P_{lsiR534}$) (Figure 1b,c). This approach mirrors that which we used to optimize the green/red and red/far red sensors.[15] To assay UirS−UirR function, we grew batch cultures of *E. coli* carrying these plasmids under saturating aTc (100 ng/mL) and IPTG (200 μM) under 1.25 μmol m^{-2} s^{-1} of 380 (UV-violet) and 526 (green) nm light (Figure S2) and measured sfGFP abundance by flow cytometry (Methods). These experiments revealed low, light-independent sfGFP expression (Figure 1d). We next performed a series of control experiments which validated that UirS, UirR (Figure S3), and PCB (Figure S4) are produced and that there is no photoxicity (Figure S5) nor aTc photodegradation (Figure S6) under these conditions. Therefore, we hypothesized that $P_{lsiR534}$ is nonfunctional in this context.

In *Synechocystis* PCC6803, *lsiR* mRNA levels are much lower than those of *csiR1*, likely due to a transcriptional terminator between the two genes.[20,21] Assuming that UirR∼P activates transcription of *lsiR* via P_{csiR1}, we hypothesized that the lack of observable $P_{lsiR534}$ activity in *E. coli* may be a result of inefficient transcriptional read-through and/or poorly understood regulation. Thus, we replaced $P_{lsiR534}$ with a 109 bp fragment containing the 108 bp *uirR/csiR1* intergenic region and the *csiR1* +1 site (hereafter $P_{csiR1\text{-}109}$) (Figure 1b,c) and measured sfGFP expression as before. Indeed, sfGFP levels increase 4.41 ± 0.04-fold from $P_{csiR1\text{-}109}$ in UV-violet versus green light (Figure 1d), suggesting that P_{csiR1} is an output promoter of UirS−UirR.

To validate that the observed UV-violet response a result of UirS−UirR signaling through $P_{csiR1\text{-}109}$, we repeated the above experiment using variants containing different deactivating mutations. In particular, we deleted *uirS*, mutated the conserved UirS histidine to a noncatalytic alanine (H658A), and mutated the conserved UirR aspartate to a nonfunctional glycine (D54G).[16] All three mutations result in low sfGFP levels and abolish UV-violet activation (Figure 1e). Deletion of the *uirR* DBD reduces sfGFP to very low levels and similarly eliminates the light response (Figure 1e). Elimination of PCB production via deletion of *ho1-pcyA* results in light-insensitive sfGFP expression (Figure 1e). Taken together, these results indicate that UV-violet light activates UirS−UirR signaling in *E. coli*.

Characterizing P_{csiR1} Functional Elements. Next, we characterized the interaction between UirR and P_{csiR1}. Sequence analysis revealed that P_{csiR1} positions −108 to −85 contain no identifiable regulatory motifs, the −84 to −74 region is A/T-rich, the −69 to −40 region contains two 11 bp direct repeats separated by an 8 bp palindrome, and there is a cyanobacterial −10 hexamer[22] upstream of the +1 (Figures 1c and S7a). As expected, deletion of −108 to −94 has little effect (Figure S7b). Further deletion of 5 bp fragments between −93 and −74 incrementally decreases sfGFP levels, with only a small effect on dynamic range (ratio of sfGFP levels in UV-violet to green light) (Figure S7b), suggesting that this region enhances transcription rate. Consistent with the 11 bp direct repeat being the UirR operator site, mutations to either half-site (Figure S8a) reduce transcription to low levels and abolish UV-violet activation (Figure S8b). Additionally, scrambling the palindrome reduces transcription and UV-violet activation to a lesser extent (Figure S8b). These results indicate that the entire 30 bp region containing the direct repeats and palindrome is involved in transcriptional activation. Finally, we engineered a synthetic repressible *E. coli* promoter where this region overlaps the −35 and −10 sites such that transcription factor binding interferes with RNA polymerase binding. This promoter is repressed strongly by UirR (Figure S9), suggesting that it binds the 11 bp direct repeat.

UirS Signals to UirR via Phosphorylation. If UirS P_{UV} was to sequester UirR and prohibit it from becoming phosphorylated, then *uirS* deletion should result in increased UirR∼P levels and increased $P_{csiR1\text{-}109}$ transcription. However, we observe that $P_{csiR1\text{-}109}$ activity is lower in *E. coli* lacking *uirS* (Figure 1e). Furthermore, the conserved UirS histidine and UirR aspartate are both required for UV-violet activation (Figure 1e), suggesting a canonical TCS phosphorylation mechanism.

Direct measurements of UirR phosphorylation *in vitro* have been unsuccessful, possibly due to the inability to purify full-length UirS.[16,17] However, the Phos-tag method[25] enables visualization of phosphorylated and unphosphorylated proteins in cell lysates[26,27] via their differential electrophoretic mobilities in acrylamide gels containing a phosphoryl group binding agent. To examine whether UirS phosphorylates UirR, we conducted Phos-tag SDS PAGE and western blots (Methods) using lysates from exponentially growing *E. coli* expressing N-terminal His-tagged UirR in the presence or absence of UirS. Indeed, we observed that the presence of UirS and UV-violet light results in a slower migrating UirR∼P band that is absent both in bacteria lacking UirS, or expressing UirS and treated with green light (Figure 2). Furthermore, the intensity of the UirR∼P band depends upon the intensity of UV-violet illumination (Figure 2). These data demonstrate that UV-violet light induces UirS to phosphorylate UirR. This conclusion is reinforced by the fact that $P_{csiR1\text{-}109}$ activity increases with increasing UirS expression (Figure S12).

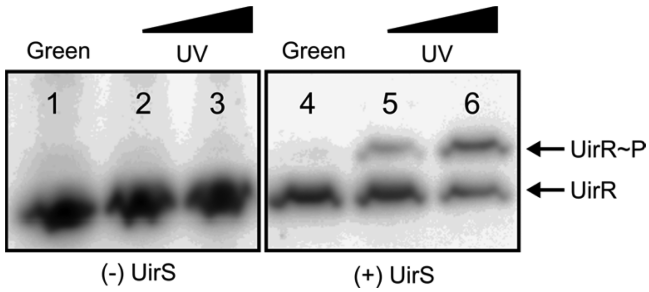

Figure 2. UirS phosphorylates UirR in a UV-violet light-dependent manner. Western blot of cellular lysates analyzed by Phos-tag gel electrophoresis. Lanes 1−3 contain lysates of BW29655/pPR219.08-N containing N-terminally His-tagged UirR exposed to (1) 34 μmol m^{-2} s^{-1} 525 nm, (2) 1 μmol m^{-2} s^{-1} 380 nm, or (3) 12 μmol m^{-2} s^{-1} 380 nm, whereas lanes 4−6 contain lysates of BW29655/pPR219.08-N/pPR161-2 containing N-terminally His-tagged UirR and UirS exposed to (4) 34 μmol m^{-2} s^{-1} 525 nm, (5) 1 μmol m^{-2} s^{-1} 380 nm, or (6) 12 μmol m^{-2} s^{-1} 380 nm. In lanes 4−6, *uirS* expression is induced from pPR161-2 with 1000 μM IPTG.

Hardwiring UirS and UirR Expression for Optogenetics. Chemical inducers are undesirable for optogenetics as they may introduce unwanted variability and make the photoreceptor incompatible with strains otherwise responsive to them.[2,15] Therefore, we replaced the inducible *uirS* and *uirR* promoters with a small library of constitutive versions of different strengths and screened for the combination yielding the largest dynamic range (Figure S13). The best performing combination (encoded on plasmids pPR220.08 and

DOI: 10.1021/acssynbio.6b00068
ACS Synth. Biol. 2016, 5, 733−740

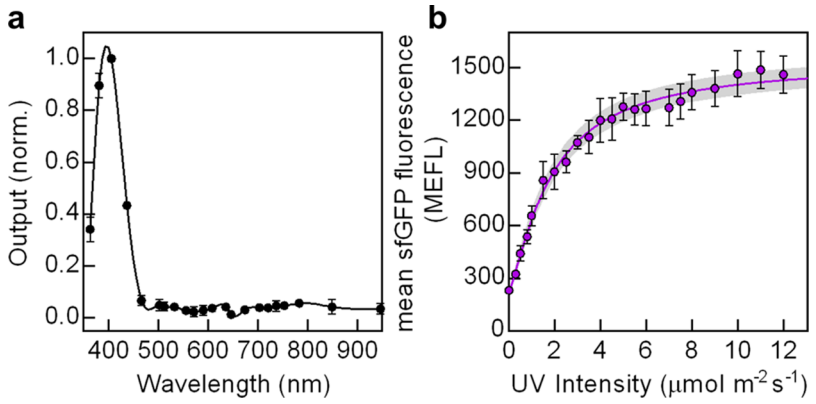

Figure 3. UirS−UirR action spectrum and steady-state transfer function. (a) Normalized response of hardwired UirS−UirR to 0.8 μmol m^{-2} s^{-1} light emitted from LEDs with peak wavelengths spanning 361−947 nm. Markers and error bars are the mean and SEM of n = 3 experiments performed in three separate illumination devices on 1 day. A cubic spline interpolation (solid line) is shown as a guide to the eye. (b) sfGFP fluorescence of UirS−UirR illuminated with 0−12 μmol m^{-2} s^{-1} of 380 nm light, with green light held constant at 0.5 μmol m^{-2} s^{-1}. The data is fit via nonlinear least-squares regression (Methods) to the activating form of the Hill equation, $b + \frac{aI^n}{k^n + I^n}$, where I is the intensity of UV-violet light in μmol m^{-2} s^{-1} and the parameter best fit values plus or minus the standard error are b = 227.6 ± 9.6 MEFL, a = 1324 ± 54 MEFL, k = 1.88 ± 0.16 μmol m^{-2} s^{-1}, and n = 1.31 ± 0.08. The best fit is shown (solid line) along with the gray envelope representing the interquartile range of 500 simulations produced by randomly sampling the measured parameter uncertainties. Markers and error bars are the mean and SEM of n = 3 experiments performed on separate days.

pPR219.05) gives rise to a better dynamic range (6.24 ± 0.24-fold; Figure S13b) and faster doubling time (Figure S14) than those of the original system. We therefore used this "hardwired" plasmid system for all subsequent experiments.

Characterizing the UirS−UirR Action Spectrum. The UirS GAF (cGMP-specific phosphodiesterases, adenylyl cyclases, and FhlA) subdomain responsible for light absorption shows narrow activation by UV-violet light *in vitro*.[16,17,19] However, this absorption spectrum may not directly reflect the *in vivo* action spectrum, or relationship between input wavelength and transcriptional output for the full UirS−UirR pathway. Therefore, we measured the action spectrum by exposing our engineered *E. coli* to 0.8 μmol m^{-2} s^{-1} total photon flux from each of 22 different light emitting diodes (LEDs) with peak emission wavelengths spanning 361−947 nm (Methods; Table S1). Consistent with the *in vitro* data, 380 and 405 nm LEDs most strongly activate the system, 361 and 430 nm LEDs result in intermediate activation, and all other LEDs result in no response (Figure 3a). Cubic spline interpolation reveals that the system is activated to greater than 50% of its maximal response by a relatively narrow window between 370 and 434 nm (Figure 3a).

Characterizing and Modeling the UirS−UirR Steady-State Transfer Function. We next measured the steady-state response, or transfer function, of UirS−UirR to increasing intensities of UV-violet light in the presence of different amounts of green. Without green light, sfGFP follows an activating Hill-like response with increasing UV-violet intensity up to 12 μmol m^{-2} s^{-1} (Figure S15; k = 0.97 ± 0.04 μmol m^{-2} s^{-1} and n = 1.35 ± 0.05). At higher intensities, the growth rate of *E. coli* begins to slow. Addition of 0.5 μmol m^{-2} s^{-1} green reduces UirS−UirR sensitivity (k = 1.88 ± 0.16 μmol m^{-2} s^{-1}) but maintains the shape of the transfer function (n = 1.31 ± 0.08) (Figure 3b). Higher green intensities reduce the sfGFP levels reached at 12 μmol m^{-2} s^{-1} UV-violet and thus the dynamic range (Figure S16). We therefore performed all subsequent experiments with constant 0.5 μmol m^{-2} s^{-1} green and variable UV-violet.

Characterizing and Modeling UirS−UirR Response Dynamics. To characterize UirS−UirR activation dynamics, we preconditioned four groups of cells in green light, resulting in low gene expression, and then increased UV-violet to the intensities resulting in 25, 50, 75, and 100% maximal output (Figure 3b) in a single step and tracked sfGFP levels over time (Methods) (Figures 4a and S17a−d). We characterized deactivation dynamics by preconditioning cells in 12 μmol m^{-2} s^{-1} UV-violet plus green and reduced UV-violet to the intensities resulting in 75, 50, and 25% and minimal output (Figures 4b and S17e−h). We fit the resulting data to the same phenomenological model of TCS dynamics used for the green/red and red/far red sensors[2] (Figure S18) (Methods). The model contains a term for a pure delay after the light step change wherein sfGFP production rate does not change (τ) and variables for sfGFP production rate (p) and abundance (g) that vary as first-order exponential processes with rate parameters k_p^{on} (for step increases in UV-violet) or k_p^{off} (for step decreases) and k_g (the cell growth rate). The steady state reached by the system depends on UV-violet intensity and is described by the Hill function (Figure 3b). For both activation and deactivation, τ = 6.82 ± 0.38 min. After this delay, p switches with k_p^{on} = 0.294 ± 0.106 min^{-1} ($t_{1/2}$ = 2.36 ± 0.86 min) and k_p^{off} = 0.086 ± 0.012 min^{-1} ($t_{1/2}$ = 8.06 ± 1.12 min). k_g is fixed at 0.0203 min^{-1} on the basis of the measured cell growth rate. All fit parameters and the standard error in their estimation are listed in Tables S2 and S3.

Predictive Control of UirS−UirR Gene Expression Dynamics. To program tailor-made gene expression signals, we combined the above dynamical model with our previous light program generator algorithm.[2] As a reference, we specified a complex waveform spanning 8 h that contains linear increases and decreases, a sinusoid, and constant gene expression levels (Figure 5). We have previously programmed the green/red and red/far red sensor output dynamics using a similar signal.[2] The root-mean-squared errors ($RMSE_{REF}$) between the reference waveform and experimental data for those sensors are 4.83 and 5.9%, expressed as a percentage of the output range of each system.[2] The light program generator produces a UV-violet

DOI: 10.1021/acssynbio.6b00068
ACS Synth. Biol. 2016, 5, 733−740

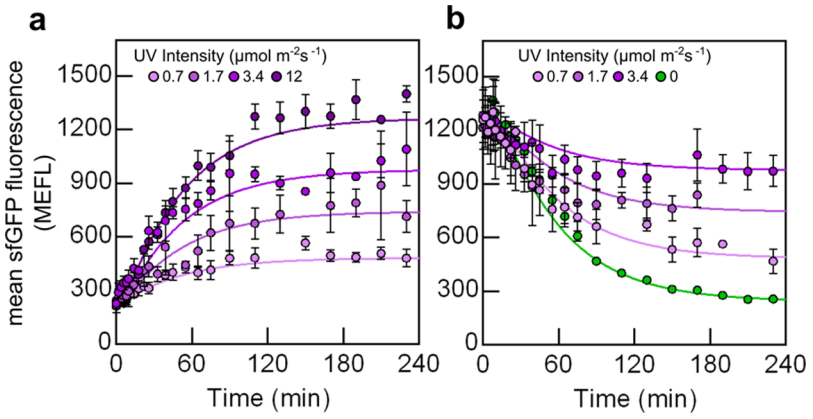

Figure 4. Response of UirS−UirR to step changes in UV-violet light intensity. (a) Response to a step increase in UV-violet light from 0 to 0.7, 1.7, 3.4, or 12 μmol m^{-2} s^{-1}. (b) Response of UirS−UirR to a step decrease in UV-violet light from 12 μmol m^{-2} s^{-1} to 0.7, 1.7, 3.4, or 0 μmol m^{-2} s^{-1}. In all experiments, green light is held constant at 0.5 μmol m^{-2} s^{-1}. Cells are preconditioned for 4 h in 0 (a) or 12 μmol m^{-2} s^{-1} (b) of UV-violet light. The data is fit via nonlinear least-squares regression to the kinetic model of gene expression (Methods), and the sfGFP fluorescence best fit (solid line) is shown. The individual curves from each experiment are shown in Figure S17. Markers and error bars represent the mean and SEM of n = 2 or more experiments.

light time course predicted to drive sfGFP levels to closely follow the reference (Figure 5). Exposure of *E. coli* expressing UirS−UirR to this light signal drives sfGFP levels to track the waveform closely ($RMSE_{REF}$ 8.16%; Figure 5). The experimental data lag slightly behind the simulated response for initial increases in sfGFP (Figure 5), suggesting that τ or k_p^{on} may be underestimated, a challenge that can be readily overcome with additional parametrization experiments.[2] These results clearly demonstrate that we have captured the input/output dynamics of UirS−UirR and that this TCS can be deployed as a high-performance optogenetic tool for programming gene expression.

Conclusions. UirS−UirR offers several benefits for optogenetics. First, it is activated exclusively by UV-violet light. This narrow action spectrum contrasts a previous blue-shifted system based upon the nonphotoreversible YtvA light oxygen voltage (LOV) sensor domain[28,29] that absorbs strongly between 375 and 490 nm.[30] Additionally, UirS−UirR responds to changes in light in approximately 10 min, much faster than the >2 h response time of the YtvA-based systems.[29] We have exploited these rapid dynamics to program a challenging gene expression signal with high predictability. Due to its narrow UV-violet action spectrum, photoreversibility, and fast dynamics, UirS−UirR should be ideal for multiplexing with our previous green/red and red/far red sensors. A three-input, three-output photoreversible TCS system could enable dynamical control of three sets of genes independently, a powerful technology for characterization of multicomponent cellular pathways[31] or rapid optimization of multienzyme engineered metabolic pathways.[32]

The fact that UirR~P activates transcription from P_{csiR1} suggests that *csiR1* and *lsiR* are induced in UV-violet light in *Synechocystis* PCC6803. However, what role, if any, *csiR1* plays in UV-violet negative phototaxis remains unknown. Additionally, the pathway by which high C_i reduces *csiR1-lsiR* transcription is not known.[21] Although UirS encodes a functional ethylene binding domain[33] and CO_2 likely interferes with ethylene binding at this domain,[34] it has not been implicated in C_i signaling. It is therefore possible that UirS senses UV and green light as well as ethylene and C_i. Our *E. coli* system could be used to directly examine how these inputs affect UirS−UirR signaling individually and in combination,

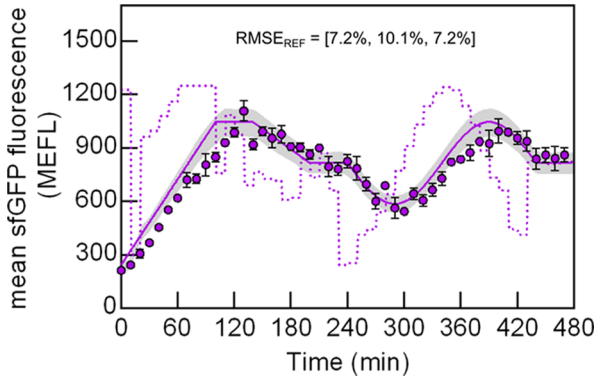

Figure 5. Biological function generation with UirS−UirR. Reference gene expression signal (solid line), the control light signal used to generate the reference waveform transformed into fluorescence units through the steady-state transfer function of UirS−UirR (dotted line), and the experimental data with markers and error bars representing the mean and SEM of n = 2 or more experiments are shown. To generate the dotted line, the UV-violet intensity was transformed into sfGFP (MEFL) units using the best fit data from Figure 3b. The model-predicted response of the system is shown as the interquartile range of 500 simulations in gray as in Figure 3b. $RMSE_{REF}$ is calculated for each experimental replicate.

without regulatory cross-talk from cyanobacterial networks. Furthermore, both bacteria[35] and yeast[36] have been engineered to synthesize ethylene, a freely diffusible gas. Our UirS−UirR system could be combined with ethylene production to engineer new cell−cell communication systems capable of rapid, long distance signaling (over an estimated 10 cm in under 15 min.).[37]

UirS is a member of a group of CBCRs containing a conserved DXCF motif (X is any amino acid) within the bilin-binding GAF domain.[16] DXCF CBCRs have a remarkable diversity[10] of spectral response properties, and variants with similar photocycles cluster in phylogenetic groups based on GAF domain sequence.[38] Although the spectral responses of a set of green/blue and blue/orange groups can be predicted from their primary amino acid sequence,[38] the sequence determinants of function in this family of sensors remains incompletely understood. One major limitation is that the

DOI: 10.1021/acssynbio.6b00068
ACS Synth. Biol. 2016, 5, 733−740

predominant method for studying DXCF CBCRs is to heterologously express and purify them and analyze their spectral properties *in vitro*, a relatively low-throughput method. To investigate how different primary sequence elements impact photocycle in this diverse family using this method, one would need to purify and characterize the spectral responses of dozens or more mutants, an expensive and laborious process. By contrast, the system reported in this article constitutes the first DXCF CBCR to be moved to plasmids and linked to fluorescent reporter gene output in a rapidly growing laboratory organism. One could combine standard methods for creating large plasmid-based mutant libraries with different color light inputs and high-throughput cell sorting to more readily identify mutants that impart new wavelength specificities. Thus, our *E. coli* UirS−UirR system could be used to study how primary sequence affects photobiology with much higher throughput than current methods.

METHODS

Plasmids, Strains, and Media. All plasmids were constructed by Golden Gate cloning.[39] NEB 10-β (New England Biolabs, cat no. C3019H) was used for cloning. The *uirSR* operon and $P_{lsiR534}$ were amplified from *Synechocystis* PCC6803 genomic DNA. pSR41.3 and pSR34[15] were used as the template vectors for the construction of pPR157-1 and pPR161-2, respectively. To construct pPR164-1, we deleted the 425 bp downstream of the *csiR1* start site in $P_{lsiR534}$ in pPR157-1 and replaced the sRBS upstream of *sfgfp* with an sRBS designed for $P_{csiR1\text{-}109}$ with a predicted strength of 17 190 au.[40] For constitutive UirS and UirR expression, we first identified 11 promoters (Figure S13a) from the Anderson (http://parts.igem.org/Promoters/Catalog/Anderson) and BIOFAB[41] collections (http://biofab.synberc.org/data) that are expected to generate a wide range of expression levels. We ordered single-stranded oligonucleotides encoding each promoter and annealed them to generate phosphorylated double-stranded fragments with sticky ends (5′: CTGA; 3′: CAGT). We then used PCR to seamlessly delete the *tetR* and *lacI* expression cassettes from pPR164-1 and pPR161-2 and replaced the sRBSs upstream of *uirR* and *uirS* with BCD22 and apFAB655.[41] Next, we replaced $P_{LTetO\text{-}1}$ in pPR164-1 with constitutive promoters to generate pPR219.01−pPR219.11 encoding the UirR expression library. We replaced P_{tac} in pPR161-2 with constitutive promoters to generate pPR220.01−pPR220.11 encoding the UirS expression library. To enable immunodetection on a western blot, a 6×-His tag along with a short flexible linker (-GSG-) was added to the N-terminus of UirR on pPR219.08 to yield pPR219.08-N. Table S4 describes all plasmids used in this study. Primers were ordered from IDT, and DNA sequencing was performed either at GENEWIZ, NJ, or Lone Star Laboratories, Houston, TX. NEB 10-β strains were grown in LB media supplemented with appropriate antibiotics.

All experiments were performed in *E. coli* BW29655 (BW28357 Δ*(envZ-ompR)520(::FRT)*)[42] obtained from CGSC, Yale University. Sequence-verified plasmids were transformed into chemically competent BW29655, and isolated clones were picked and grown to exponential phase (OD_{600} < 0.2) in LB media supplemented with appropriate antibiotics. Filter-sterilized glycerol was added to a final concentration of 20% (v/v), and the OD_{600} was recorded prior to aliquoting 50 μL of cells into PCR tubes and freezing at −80 °C. Unless otherwise stated, all experiments were started from individual aliquots of cultures frozen at exponential phase.

Experiments were conducted in M9 minimal media (1× M9 salts, 0.4% w/v glucose, 0.2% w/v casamino acids, 2 mM MgSO4, 100 μM $CaCl_2$) supplemented with appropriate antibiotics (chloramphenicol at 34 μg/mL and spectinomycin at 100 μg/mL, unless specified).

Phos-Tag SDS PAGE and Western Blot. Cellular lysate was prepared as described previously[27] with the following modifications. Exponentially growing culture (3 mL; OD_{600} < 0.2) was centrifuged at 10 000*g* for 2 min, and the pellet was gently resuspended in 55 μL of 1× BugBuster and 0.1% Lysonase (EMD-Millipore, cat. no. 713703), followed by the addition of 18 μL of 4× Laemmli sample buffer (Bio-Rad, cat. no. 1610747) and gentle vortexing to mix. Samples were immediately flash frozen in liquid nitrogen and thawed on ice prior to electrophoresis. 25 μL of sample was loaded into each well of precast 12.5% SuperSep Phos-Tag polyacrylamide gels (cat. no. 195-17991, Wako Chemicals, USA), and electrophoresis was performed at 35 mA for 60 min, according to the manufacturer's recommendations. The gel was washed with gentle agitation in transfer buffer (25 mM Tris, 192 mM glycine, 10% methanol) containing 1 mM EDTA twice for 15 min each, followed by two 15 min washes in transfer buffer without EDTA. Gel transfer to a PVDF membrane was performed in an XCell SureLock Mini-Cell (Invitrogen) at 30 V for 90 min at room temperature. Following transfer, the PVDF membrane was blocked in 5% non-fat milk in PBS-T (phosphate buffered saline containing 0.1% Tween 20) for 60 min and subsequently incubated with primary anti-His antibody (ARP, cat. no. 02-9002) diluted 1:1000 in PBS-T containing 3% bovine serum albumin (BSA) for 90 min at room temperature. After several washes in PBS-T, the PVDF membrane was incubated in secondary anti-mouse horseradish peroxidase (HRP)-conjugated antibody (Jackson Immunoresearch, cat. no. 111-035-144) diluted 1:10 000 in PBS-T containing 3% BSA for 60 min at room temperature. Following secondary antibody incubation, the PVDF membrane was washed in PBS-T, and chemiluminescent immunodetection was performed using Clarity western ECL substrate (Bio-Rad, cat. no. 1705061) according to the manufacturer's recommendations. PVDF membrane imaging was carried out on an ImageQuant LAS4000.

Optical Hardware. All optogenetic experiments were performed in two custom 24-well plate compatible LED-based devices mounted in a 37 °C, 250 rpm shaking incubator. The LED intensities in each well were calibrated to one another using a fiber-optic spectrophotometer (StellarNet cat. no. EPP2000 UVN-SR-25 LT-16), and the calibration was validated by measuring the 50% response of BW29655/pPR220.08/pPR219.05 to UV-violet or UV-violet and green light. On the basis of the validation, we observed that the leftmost column of wells was miscalibrated and discarded data collected from these wells. To minimize systematic errors that could result from unevenly calibrated LED intensity in each well, replicates of each experimental data point were randomized or assigned to different wells.

Optogenetic Experiments. A frozen PCR tube aliquot containing the desired strain of cells was thawed at the bench for 1.5 min and inoculated into M9 media containing appropriate antibiotics at an OD_{600} of 1×10^{-4} for chemical-inducible strains and 1×10^{-5} for hardwired strains. Starting densities were chosen such that at the end of an 8 h experiment

DOI: 10.1021/acssynbio.6b00068
ACS Synth. Biol. 2016, 5, 733−740

the cells would be at steady state and in exponential phase (OD_{600} < 0.2). Cells were supplemented with aTc (Clonetech cat. no. 631310) and IPTG (VWR cat. no. 14213-263) when necessary. M9 media (500 μL) containing cells was aliquoted into each well of clear-bottom polystyrene plates (Krystal, ArcticWhite, cat. no. AWLS-303008). The plates were sealed with optically insulating aluminum foil (VWR cat. no. 60941-126) and placed in the 24-well plate device programmed with the desired light exposure program. Step response dynamics experiments were performed using a staggered-start method.[2] Cells were grown for 8 h at 37 °C with shaking at 250 rpm. Plates were then extracted from the 24-well plate devices and iced for 20 min in an ice−water slurry to arrest growth. Sample (100 μL) contained in each well was transferred to cytometer tubes containing chilled PBS + 500 μg/mL rifampicin and transferred to a 37 °C water bath for 1 h. This step allows maturation of translated sfGFP while preventing the transcription of new *sfgfp* mRNA.[2] Cells were then transferred to an ice−water bath for 15 min before fluorescence was measured via flow cytometry.

Flow Cytometry and Data Analysis. Flow cytometry was performed using a BD FACScan flow cytometer.[2] Cells were typically acquired at 1000−1500 events/second at the instrument settings specified in Table S5. A standard acquisition gate based on typical FSC/SSC values seen for *E. coli* cells was specified, and 20 000 events were acquired for each sample within this gate. Rainbow calibration beads from Spherotech, Inc. (cat. no. RCP-30-20A) were measured every day at the same detector gain settings. After acquisition, the raw flow cytometry data was processed using FlowCal.[43] First, a standard curve was generated using calibration beads that converts the arbitrary fluorescence units reported by the flow cytometer into MEFL. The first 250 and the last 100 time-ordered events for each sample were discarded, since these acquisition events are subject to uneven sample tube pressurization. A gate was drawn around the densest region of FSC vs SSC values, retaining 50% (or 10 000 events on average) per sample. Finally, the arbitrary fluorescence units for each event were transformed into corresponding MEFL values using the standards curve, and the arithmetic mean of all of the events was calculated and reported as the population mean of the entire sample. Representative histograms from all figures in the main text are shown (Figure S19)

Hill Function Model Fitting. Model fitting was performed using the nonlinear least-squares curve-fitting package available in GraphPad Prism, version 6.00, for Windows, GraphPad Software, La Jolla, CA. SEM was calculated across three experimental replicates at each intensity i to assign an estimated uncertainty in measurement to each data point. The data was weighted by this estimate $\left(w_i = \frac{1}{\mathrm{SEM}_i^2}\right)$ before being fit to the activating form of the Hill function.

Dynamical Model Fitting. Dynamical model fitting was performed using the nonlinear least-squares curve-fitting package available in GraphPad Prism. The SEM was first calculated across n = 2 or more replicates at every time point for each step−response curve. This SEM was then used to weight individual data points as described above. The data was fit to the analytical solution of the step-change model of gene expression[2] (Figure S18). The delay parameter τ was fit globally to all data, whereas rate parameters k_p^{on} and k_p^{off} were shared by the step-on and step-off curves, respectively. Since we observed daily variation in the fluorescence levels of the data (Figure S17), we allowed the steady-state Hill function parameters a and b to float for every curve; however, n and k were assigned the best-fit values from the steady-state transfer function in Figure 3b. The estimated a and b for each step−response curve is listed in Table S3. The predictive model uses the mean of the fit a and b values, weighted by the uncertainty in their estimation. All estimated fit parameters along with the standard error in their estimation are listed in Table S2.

Gene Expression Programming. Light program computation and model simulations were performed using previous scripts.[2] The scripts were modified to accommodate the UirS−UirR model and are provided in the Supporting Information.

■ ASSOCIATED CONTENT

Supporting Information

The Supporting Information is available free of charge on the ACS Publications website at DOI: 10.1021/acssynbio.6b00068.

Figures and tables supporting main figures, results and discussion (PDF)

■ AUTHOR INFORMATION

Corresponding Author

*E-mail: jeff.tabor@rice.edu.

Notes

The authors declare no competing financial interest.

■ ACKNOWLEDGMENTS

We thank Sebastian Schmidl for providing plasmids, Karl Gerhardt and other members of the Tabor lab for assistance with optogenetic hardware, Evan Olson for assistance with modeling and light program generation, and Sebastian Castillo Hair for assistance with flow cytometry data analysis. We thank Lucas Hartsough, Oleg Igoshin, Evan Olson, and anonymous reviewers for helpful comments on the manuscript. This work was supported by the National Science Foundation (EFRI-1137266), The Office of Naval Research (MURI N000141310074), and the Welch Foundation (C-1856). Plasmids will be available from Addgene.

■ ABBREVIATIONS

TCS, two-component system; SK, sensor kinase; RR, response regulator; CBCR, cyanobacteriochrome; GAF domain, cGMP-specific phosphodiesterase, adenylyl cyclase FhlA-containing domain; Phy, phytochrome; PCB, phycocyanobilin

■ REFERENCES

(1) Olson, E. J., and Tabor, J. J. (2014) Optogenetic characterization methods overcome key challenges in synthetic and systems biology. *Nat. Chem. Biol. 10*, 502−11.

(2) Olson, E. J., Hartsough, L. A., Landry, B. P., Shroff, R., and Tabor, J. J. (2014) Characterizing bacterial gene circuit dynamics with optically programmed gene expression signals. *Nat. Methods 11*, 449−55.

(3) Toettcher, J. E., Weiner, O. D., and Lim, W. A. (2013) Using Optogenetics to Interrogate the Dynamic Control of Signal Transmission by the Ras/Erk Module. *Cell 155*, 1422−1434.

(4) Imayoshi, I., Isomura, A., Harima, Y., Kawaguchi, K., Kori, H., Miyachi, H., Fujiwara, T., Ishidate, F., and Kageyama, R. (2013) Oscillatory control of factors determining multipotency and fate in mouse neural progenitors. *Science 342*, 1203−8.

(5) Deisseroth, K. (2015) Optogenetics: 10 years of microbial opsins in neuroscience. *Nat. Neurosci. 18*, 1213−1225.

DOI: 10.1021/acssynbio.6b00068
ACS Synth. Biol. 2016, 5, 733−740

(6) Gao, R., and Stock, A. M. (2009) Biological insights from structures of two-component proteins. *Annu. Rev. Microbiol. 63*, 133–54.
(7) Psakis, G., Mailliet, J., Lang, C., Teufel, L., Essen, L.-O., and Hughes, J. (2011) Signaling kinetics of cyanobacterial phytochrome Cph1, a light regulated histidine kinase. *Biochemistry 50*, 6178–88.
(8) Rockwell, N. C., and Lagarias, J. C. (2010) A brief history of phytochromes. *ChemPhysChem 11*, 1172–80.
(9) Rockwell, N. C., Su, Y.-S., and Lagarias, J. C. (2006) Phytochrome structure and signaling mechanisms. *Annu. Rev. Plant Biol. 57*, 837–58.
(10) Rockwell, N. C., Martin, S. S., Feoktistova, K., and Lagarias, J. C. (2011) Diverse two-cysteine photocycles in phytochromes and cyanobacteriochromes. *Proc. Natl. Acad. Sci. U. S. A. 108*, 11854–9.
(11) Rockwell, N. C., Martin, S. S., Gan, F., Bryant, D. A., and Lagarias, J. C. (2015) NpR3784 is the prototype for a distinctive group of red/green cyanobacteriochromes using alternative Phe residues for photoproduct tuning. *Photochem. Photobiol. Sci. 14*, 258–69.
(12) Levskaya, A., Chevalier, A. A., Tabor, J. J., Simpson, Z. B., Lavery, L. A., Levy, M., Davidson, E. A., Scouras, A., Ellington, A. D., Marcotte, E. M., and Voigt, C. A. (2005) Synthetic biology: engineering Escherichia coli to see light. *Nature 438*, 441–2.
(13) Tabor, J. J., Levskaya, A., and Voigt, C. A. (2011) Multichromatic control of gene expression in Escherichia coli. *J. Mol. Biol. 405*, 315–24.
(14) Tabor, J. J., Salis, H. M., Simpson, Z. B., Chevalier, A. A., Levskaya, A., Marcotte, E. M., Voigt, C. a, and Ellington, A. D. (2009) A synthetic genetic edge detection program. *Cell 137*, 1272–81.
(15) Schmidl, S. R., Sheth, R. U., Wu, A., and Tabor, J. J. (2014) Refactoring and optimization of light-switchable Escherichia coli two-component systems. *ACS Synth. Biol. 3*, 820–31.
(16) Song, J.-Y., Cho, H. S., Cho, J.-I., Jeon, J.-S., Lagarias, J. C., and Park, Y.-I. (2011) Near-UV cyanobacteriochrome signaling system elicits negative phototaxis in the cyanobacterium Synechocystis sp. PCC 6803. *Proc. Natl. Acad. Sci. U. S. A. 108*, 10780–5.
(17) Narikawa, R., Suzuki, F., Yoshihara, S., Higashi, S. -i., Watanabe, M., and Ikeuchi, M. (2011) Novel Photosensory Two-Component System (PixA-NixB-NixC) Involved in the Regulation of Positive and Negative Phototaxis of Cyanobacterium Synechocystis sp. PCC 6803. *Plant Cell Physiol. 52*, 2214–2224.
(18) Kwon, J., Oh, J., Park, C., Cho, K., Kim, S. I., Kim, S., Lee, S., Bhak, J., Norling, B., and Choi, J.-S. (2010) Systematic cyanobacterial membrane proteome analysis by combining acid hydrolysis and digestive enzymes with nano-liquid chromatography-Fourier transform mass spectrometry. *J. Chromatogr. A 1217*, 285–293.
(19) Ulijasz, A. T., Cornilescu, G., von Stetten, D., Cornilescu, C., Velazquez Escobar, F., Zhang, J., Stankey, R. J., Rivera, M., Hildebrandt, P., and Vierstra, R. D. (2009) Cyanochromes are blue/green light photoreversible photoreceptors defined by a stable double cysteine linkage to a phycoviolobilin-type chromophore. *J. Biol. Chem. 284*, 29757–72.
(20) Kopf, M., Klähn, S., Scholz, I., Matthiessen, J. K. F., Hess, W. R., Voß, B., Klahn, S., Scholz, I., Matthiessen, J. K. F., Hess, W. R., and Voss, B. (2014) Comparative Analysis of the Primary Transcriptome of Synechocystis sp. PCC 6803. *DNA Res. 21*, 527–539.
(21) Klähn, S., Orf, I., Schwarz, D., Matthiessen, J. K. F., Kopka, J., Hess, W. R., and Hagemann, M. (2015) Integrated Transcriptomic and Metabolomic Characterization of the Low-Carbon Response Using an ndhR Mutant of Synechocystis sp. PCC 6803. *Plant Physiol. 169*, 1540–1556.
(22) Mitschke, J., Georg, J., Scholz, I., Sharma, C. M., Dienst, D., Bantscheff, J., Voss, B., Steglich, C., Wilde, A., Vogel, J., and Hess, W. R. (2011) An experimentally anchored map of transcriptional start sites in the model cyanobacterium Synechocystis sp. PCC6803. *Proc. Natl. Acad. Sci. U. S. A. 108*, 2124–9.
(23) Wang, H.-L., Postier, B. L., and Burnap, R. L. (2004) Alterations in global patterns of gene expression in Synechocystis sp. PCC 6803 in response to inorganic carbon limitation and the inactivation of ndhR, a LysR family regulator. *J. Biol. Chem. 279*, 5739–51.
(24) Pédelacq, J.-D., Cabantous, S., Tran, T., Terwilliger, T. C., and Waldo, G. S. (2006) Engineering and characterization of a superfolder green fluorescent protein. *Nat. Biotechnol. 24*, 79–88.
(25) Kinoshita, E., Kinoshita-Kikuta, E., and Koike, T. (2009) Separation and detection of large phosphoproteins using Phos-tag SDS-PAGE. *Nat. Protoc. 4*, 1513–21.
(26) Barbieri, C. M., and Stock, A. M. (2008) Universally applicable methods for monitoring response regulator aspartate phosphorylation both in vitro and in vivo using Phos-tag-based reagents. *Anal. Biochem. 376*, 73–82.
(27) Gao, R., and Stock, A. M. (2013) Probing kinase and phosphatase activities of two-component systems in vivo with concentration-dependent phosphorylation profiling. *Proc. Natl. Acad. Sci. U. S. A. 110*, 672–7.
(28) Möglich, A., Ayers, R. A., and Moffat, K. (2009) Design and signaling mechanism of light-regulated histidine kinases. *J. Mol. Biol. 385*, 1433–44.
(29) Ohlendorf, R., Vidavski, R. R., Eldar, A., Moffat, K., and Möglich, A. (2012) From dusk till dawn: one-plasmid systems for light-regulated gene expression. *J. Mol. Biol. 416*, 534–42.
(30) Losi, A., Polverini, E., Quest, B., and Gärtner, W. (2002) First evidence for phototropin-related blue-light receptors in prokaryotes. *Biophys. J. 82*, 2627–34.
(31) Alon, U. (2006) *An Introduction to Systems Biology: Design Principles of Biological Circuits*, CRC Press.
(32) Bartl, M., Kötzing, M., Schuster, S., Li, P., and Kaleta, C. (2013) Dynamic optimization identifies optimal programmes for pathway regulation in prokaryotes. *Nat. Commun. 4*, 2243.
(33) Rodríguez, F. I., Esch, J. J., Hall, A. E., Binder, B. M., Schaller, G. E., and Bleecker, A. B. (1999) A copper cofactor for the ethylene receptor ETR1 from Arabidopsis. *Science 283*, 996–998.
(34) Sisler, E. C. (1979) Measurement of Ethylene Binding in Plant Tissue. *Plant Physiol. 64*, 538–542.
(35) Digiacomo, F., Girelli, G., Aor, B., Marchioretti, C., Pedrotti, M., Perli, T., Tonon, E., Valentini, V., Avi, D., Ferrentino, G., Dorigato, A., Torre, P., Jousson, O., Mansy, S. S., and Del Bianco, C. (2014) Ethylene-producing bacteria that ripen fruit. *ACS Synth. Biol. 3*, 935–8.
(36) Pirkov, I., Albers, E., Norbeck, J., and Larsson, C. (2008) Ethylene production by metabolic engineering of the yeast Saccharomyces cerevisiae. *Metab. Eng. 10*, 276–80.
(37) Elliott, R. W., and Watts, H. (1972) Diffusion of some Hydrocarbons in Air: a Regularity in the Diffusion Coefficients of a Homologous Series. *Can. J. Chem. 50*, 31–34.
(38) Rockwell, N. C., Martin, S. S., and Lagarias, J. C. (2015) Identification of DXCF cyanobacteriochrome lineages with predictable photocycles. *Photochem. Photobiol. Sci. 14*, 929–41.
(39) Engler, C., Kandzia, R., and Marillonnet, S. (2008) A one pot, one step, precision cloning method with high throughput capability. *PLoS One 3*, e3647.
(40) Espah Borujeni, A., Channarasappa, A. S., and Salis, H. M. (2014) Translation rate is controlled by coupled trade-offs between site accessibility, selective RNA unfolding and sliding at upstream standby sites. *Nucleic Acids Res. 42*, 2646–59.
(41) Mutalik, V. K., Guimaraes, J. C., Cambray, G., Lam, C., Christoffersen, M. J., Mai, Q.-A., Tran, A. B., Paull, M., Keasling, J. D., Arkin, A. P., and Endy, D. (2013) Precise and reliable gene expression via standard transcription and translation initiation elements. *Nat. Methods 10*, 354–60.
(42) Zhou, L., Lei, X.-H., Bochner, B. R., and Wanner, B. L. (2003) Phenotype MicroArray Analysis of Escherichia coli K-12 Mutants with Deletions of All Two-Component Systems. *J. Bacteriol. 185*, 4956–4972.
(43) Castillo-Hair, S. M., Sexton, J. T., Landry, B., Olson, E. J., Igoshin, O. A., and Tabor, J. J. (2016) FlowCal: A user-friendly, open source software tool for automatically converting flow cytometry data from arbitrary to calibrated units. *ACS Synth. Biol.*, DOI: 10.1021/acssynbio.5b00284.

DOI: 10.1021/acssynbio.6b00068
ACS Synth. Biol. 2016, 5, 733–740